# *Fusion protein EWS-FLI1 is incorporated into a protein granule in cells*

*Nasiha S. Ahmed*[1], *Lucas M. Harrell*[2], *Jacob C. Schwartz*[2*]

[1] Department of Molecular and Cellular Biology, The University of Arizona, Tucson, AZ 85719

[2] Department of Chemistry and Biochemistry, The University of Arizona, Tucson, AZ 85719

* Corresponding author: jcschwartz@email.arizona.edu

Keywords: Ewing sarcoma, fusion proteins, phase separation, granules, transcription

**ABSTRACT**

Ewing sarcoma is driven by fusion proteins containing a low complexity (LC) domain that is intrinsically disordered and a powerful transcriptional regulator. The most common fusion protein found in Ewing sarcoma, EWS-FLI1, takes its LC domain from the RNA-binding protein EWSR1 (Ewing Sarcoma RNA-binding protein 1) and a DNA-binding domain from the transcription factor FLI1 (Friend Leukemia Virus Integration 1). EWS-FLI1 binds RNA polymerase II (RNA Pol II) and can self-assemble through a process known as phase separation. The ability of self-oligomerizing RNA-binding proteins like EWSR1 to assemble into ribonucleoprotein granules in cells has received significant attention but the role of phase separation in EWS-FLI1 activity is less understood. We investigated the intersecting roles of EWSR1 and EWS-FLI1 to control gene expression and tumorigenic cell growth in Ewing sarcoma. We also studied interactions among EWS-FLI1, EWSR1, and RNA Pol II. We applied a crosslinking approach to demonstrate the incorporation of EWSR1 and RNA Pol II into protein granules in cells. We also identified protein granules in cells associated with the fusion protein, EWS-FLI1. Interactions through the LC domain, which allow EWS-FLI1 to bind EWSR1 and RNA Pol II, were found to be required for inclusion into the cellular granules observed by TEM. The physical characterization of EWS-FLI1 assemblies reported here offers insight into a large protein assembly that may allow EWS-FLI1 to engage its wide network of protein partners while driving tumorigenesis.

## INTRODUCTION

RNA-binding proteins are key players in every step of mRNA biogenesis (Moore and Proudfoot 2009). The FET proteins are a family of highly homologous and ubiquitously expressed RNA-binding proteins comprising FUS, EWSR1, and TAF15. These proteins are predominantly nuclear and bind thousands of RNA with degenerate specificity (Schwartz et al. 2015; Ozdilek et al. 2017). Although significantly more published work has focused on the activities of FUS in cells, recent studies are shedding new light on the properties and functions of EWSR1. FET proteins contribute to regulation of expression for thousands of genes (Masuda et al. 2015; Schwartz et al. 2012). FUS and EWSR1 bind the C-terminal domain (CTD) of RNA Pol II and modulate its phosphorylation (Kwon et al. 2013; Schwartz et al. 2013; Gorthi et al. 2018). EWSR1 has also been shown to bind a broad network of nascent RNA transcripts, RNA-processing factors, and transcription factors (Chi et al. 2018). The large number of interactions maintained by FET proteins provide a variety of avenues to influence gene expression in cells (Kawaguchi et al. 2020; Chi et al. 2018).

The FET protein genes are frequently involved in genomic translocation events in sarcomas (Riggi et al. 2007; Tan and Manley 2009). The second most common pediatric bone cancer, Ewing sarcoma, is driven by a translocation event fusing the N-terminal low complexity (LC) domain of a FET protein and the DNA-binding domain (DBD) of an ETS transcription factor. In 85% of Ewing sarcomas, the LC domain of EWSR1 is fused with the DBD from the FLI1, forming an oncogenic protein EWS-FLI1 (Delattre et al. 1992; Grünewald et al. 2018). Ewing sarcomas typically possess few mutations other than forming EWS-FLI1, which is sufficient to transform cells (Kovar et al. 1996; Tirode et al. 2014; Stewart et al. 2014). The FLI1 DBD in EWS-FLI1 recognizes a short DNA sequence, GGAA, and binds in cells to microsatellites of minimally 10 repeats of the motifs (Gangwal et al. 2008; Johnson et al. 2017; Vo et al. 2016). EWS-FLI1 binds RNA Pol II and a number of transcription factors, enhancer, and repressor complexes (Riggi et al. 2014; Boulay et al. 2017; Selvanathan et al. 2019; Theisen et al. 2016; Gorthi et al. 2018). Nevertheless, the mechanism for EWS-FLI1 to change transcription for many hundreds of genes remains vaguely characterized.

FET proteins have an ability to assemble into higher-order ribonucleoprotein (RNP) assemblies through a process commonly known as phase separation (Kato and McKnight 2018; Springhower et al. 2020; McSwiggen et al. 2019b; Wang et al. 2018; Qamar et al. 2018). RNA seeds this process, which is required for FET proteins to bind

RNA Pol II (Kwon et al. 2013; Schwartz et al. 2013). The LC domain of the FET proteins contains a repeated amino acid motif, [S/G]Y[S/G]. The aromatic sidechain of the tyrosine residues is critical for the domain to undergo phase separation (Kwon et al. 2013; Lin et al. 2017). In cells, phase separation appears to drive formation of several RNP granules, such as stress granules, processing (P)–bodies, and nucleoli (Riback et al. 2020). Recent studies offer evidence that phase separation is involved in gene transcription (Wei et al. 2020; McSwiggen et al. 2019a; Guo et al. 2019; Thompson et al. 2018). This form of transcription control could be expected to involve FET protein assemblies that bind the polymerase (Abraham et al. 2020; Chong et al. 2018; Murray et al. 2017).

The LC domain of EWS-FLI1 provides it the ability to assemble and phase separate (Chong et al. 2018; Boulay et al. 2017; Johnson et al. 2017). EWS-FLI1 binds and recruits EWSR1 to enhancer regions of the genome (Gorthi et al. 2018; Boulay et al. 2017). Proteins fused with the LC domain of EWSR1 form loose interacting assemblies in cells that also bind RNA Pol II (Chong et al. 2018). EWS-FLI1 can form homotypic self-interactions and heterotypic interactions through the LC domain (Spahn et al. 2003). Homo-oligomerization is required to stabilize EWS-FLI1 binding at GGAA microsatellites (Johnson et al. 2017). Oligomerization or phase separation seems to be required for EWS-FLI1 to control transcription and initiate transformation (Chong et al. 2018; Gorthi et al. 2018; Boulay et al. 2017; Kwon et al. 2013).

Our lab has found the FET protein FUS binds RNA Pol II in a nuclear granule during transcription in cells (Thompson et al. 2018). The importance of oligomerization to FET protein function suggests that EWS-FLI1 may also incorporate into a granule while functioning in cells. Here we investigate EWS-FLI1 associations with protein assemblies or granules in cells. We compared control of gene expression by EWSR1 and EWS-FLI1 and the influence each has on cell transformation. We employed crosslinking-based methods to study large protein assemblies associating with EWSR1 or EWS-FLI1 in cells and their physical characteristics. Our aim was characterizing assemblies incorporating the fusion protein to reveal greater understanding of the complex mechanisms used by EWS-FLI1 to direct cell transcription and transformation.

## RESULTS

### Transcript levels in Ewing sarcoma are affected by both EWSR1 and EWS-FLI1

EWSR1 and EWS-FLI1 share the same LC domain, which undergoes oligomerization for the proteins to regulate transcription (Kwon et al. 2013; Chong et al. 2018). Previous studies have shown the homotypic self-interactions by the LC domain of EWS-FLI1 to be required to affect transcription and transformation. Since EWS-FLI1 recruits EWSR1 to GGAA-rich sites along chromosomal DNA, we considered whether EWSR1 may influence EWS-FLI1 activity to repress or upregulate target genes.

We used RNA-seq to determine how many and which genes are regulated by EWSR1 or EWS-FLI1. We quantified abundances for poly-adenylated RNA transcripts in an Ewing sarcoma cell line, A673, which expresses EWS-FLI1 and EWSR1. Expression of EWS-FLI1, EWSR1, or both was knocked down using small interfering RNA (siRNA) transfections in cells (**Supplemental Table 1**). Each siRNA was selected from a screen of knockdown for 6 siRNA designs (**Figure 1A**, *top*). An siRNA specific for EWS-FLI1 (siEF) was targeted to the 3´ region of EWS-FLI1 mRNA, reducing the EWS-FLI1 transcript by 62 ± 3% compared to a control (siSCR) according to real-time PCR analysis (**Figure 1A**, *bottom*). The siRNA specific for EWSR1 (siEWSR1) reduced the EWSR1 transcript by 57 ± 6% compared with siSCR. An siRNA to knockdown both proteins (siE-EF) targeted the mRNA region in common for both transcripts and reduced EWS-FLI1 by 84 ± 2% and EWSR1 by 82 ± 4%. Non-specific changes to EWSR1 or EWS-FLI1 transcript levels was not observed for siEF or siEWSR1 (**Figure 1A**).

We quantified fold change in RNA levels after EWS-FLI1 knockdown for the transcriptomes found in common between this study and two previously published studies that employed Ewing sarcoma cells (Riggi et al. 2014; Sankar et al. 2013) (**Supplemental Table 1**). EWS-FLI1 knockdown was similar for all Ewing sarcoma datasets compared, ranging from 17% to 23% of transcript remaining for A673 and 38% remaining for another Ewing sarcoma cell line, SKNMC (**Supplemental Figure 1A**). Analysis of the top 10 thousand expressed A673 genes indicated a large number of gene transcripts cells increased (n = 1208) or decreased (n = 1295) more than 1.8-fold after our knockdown using siEF. The same analysis of published datasets found a similarly large number of gene transcripts affected through a stable EWS-FLI1 knockdown using an shRNA approach (**Supplemental Table 2**). We identified 983 genes affected by the EWS-FLI1 knockdown in all A673 datasets analyzed. Including data for SKNMC cells identified 760 genes affected in common. An earlier report identified a signature set of 148 unique genes repressed by EWS-FLI1 (Smith et al. 2006). In this study, we identified 123 of these in the expressed transcriptome, of which 111 (90%) were downregulated by EWS-FLI1 (**Figure 1B**, **Supplemental Table 2**).

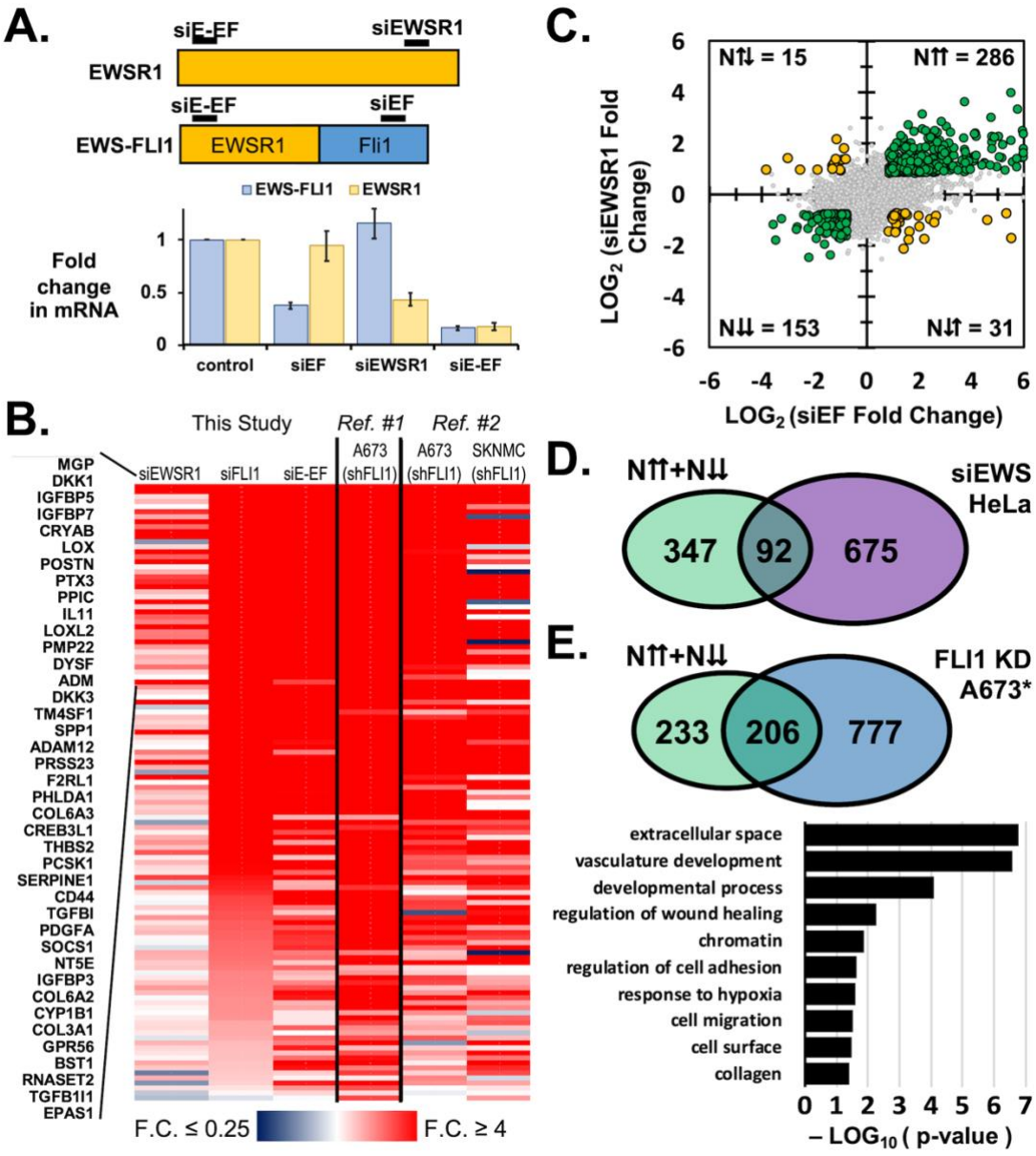


**Figure 1. A large number of transcripts respond similarly to the loss of EWS-FLI1 or EWSR1 in Ewing sarcoma.** (**A**) Schematic (*top*) shows locations in *EWSR1* or *EWS-FLI1* mRNA targeted by siRNA. Real-time PCR analysis shows average knockdown in A673 cells by siRNA transfections targeting EWS-FLI1 (siEF), EWSR1 (siEWSR1) or both (siE-EF) relative to negative controls. Error bars represent standard error about the mean. (**B**) A heat map shows fold changes for the 123 signature genes repressed by EWS-FLI1. Results are sorted according to change in the siEF treatment and genes names for the top 40 genes are listed. Published data from Ref. #1 is a stable shRNA knockdown of EWS-FLI1 in A673 cells (Sankar et al. 2013). Published data from Ref. #2 is a stable

shRNA knockdown of EWS-FLI1 in A673 or SKNMC cells (Riggi et al. 2014). (**B**) A comparison of cells treated with siEF or siEWSR1 revealed a similar increase or decrease in abundance by >1.8-fold for 439 transcripts (green) and in the opposite directions for 46 transcripts (yellow). The number of transcripts changed >1.8-fold are indicated in each quartile. (**C**) Publicly available data (GEO Accession: GSE98836) was analyzed for an EWSR1 knockdown by siRNA (siEWS) in HeLa cells. A comparison of affected HeLa gene transcripts and A673 genes shown in green for part B (N↑↑ + N↓↓) identified 92 genes changed by an EWSR1 knockdown in both cell lines, as well as for the EWS-FLI1 knockdown in A673 cells. (**D**) Genes similarly affected by siEWSR1 and siEF (N↑↑ + N↓↓) were compared to affected genes for the stable EWS-FLI1 knockdowns in A673 to identify 206 genes affected across all A673 datasets. A selection of significant Gene Ontology associations is shown from a network analysis of the 206 intersecting genes. Terms are ranked by significance, as shown by the $-LOG_{10}$ of the corrected p-values.

We next analyzed the effects of siEWSR1 in A673 cells and found fewer gene transcripts to be increased (n = 421) or decreased (n = 567). A number of affected gene transcripts were similarly upregulated by both EWSR1 and EWS-FLI1 (N↑↑ = 286) or downregulated by both (N↓↓ = 153) (**Figure 1C**, green circles). Relatively few gene transcripts were changed in opposing directions with increased levels found in the EWSR1 knockdown (N↑↓ = 15) or the EWS-FLI1 knockdown (N↓↑ = 31) (**Figure 1C**, yellow circles). We also analyzed results for knockdown of both EWSR1 and EWS-FLI1 by siE-EF. Most genes affected in both siEWSR1 and siEF (N↑↑ + N↓↓) knockdowns were also affected by the double knockdown by siE-EF (72%, n = 317, **Supplemental Table 2**).

We compared the effects of our EWSR1 knockdown to a publicly available data for an EWSR1 knockdown using siRNA transfections in a non-Ewing cell line, HeLa (GEO Accession: GSE98836) (**Supplemental Table 1**). The RNA-seq analysis indicated the knockdown of EWSR1 transcript the HeLa datasets was similar to siEWSR1 in A673 cells (**Supplemental Figure 1A**). The number of gene transcripts affected by the loss of EWSR1 was also comparable between A673 (n = 988) and HeLa (n = 767) cells. Relatively few effects were shared by A673 and HeLa (n = 112). Surprisingly, most affected genes in common between A673 and HeLa cells were also those affected by the knockdown of EWS-FLI1 in A673 cells (82%, n = 92, **Figure 1D**). This data suggests that EWSR1 does not target gene expression with a high degree of specificity. However, if a set of genes is universally targeted by EWSR1 for regulation, these may become incorporated into genes targeted by EWS-FLI1.

A previous study of an EWSR1 knockdown in A673 cells using a stable shRNA method found far fewer genes affected (Sankar et al. 2013). We repeated the analysis of this published data using the expressed transcriptome determined for this study and found 236 gene transcripts affected by the stable EWSR1 knockdown. Of these, only 26 were affected in our EWSR1 knockdown for A673 (**Supplemental Table 2**). The two studies did not differ in the level of knockdown for the EWSR1 transcript (**Supplemental Figure 1A**). A notable difference between the studies was found in the knockdown approach. The shRNA approach used by the previous report required 2 weeks of growth in culture under selection by antibiotics. We hypothesized that this difference in approach may provide sufficient time in culture to enrich for a population of cells with a substitute or alternative to dependency on the EWSR1 to recover their former EWS-FLI1 activity on gene expression.

We next applied complex network analysis to identify molecular complexes and signaling pathways in cells enriched among genes targeted by EWSR1, EWS-FLI1, or both. Our network analysis recovered previously reported associations for the 983 affected genes in common for all EWS-FLI1 knockdown datasets analyzed (Riggi et al. 2014) (**Supplemental Table 3-A**). Genes repressed by EWS-FLI1 were enriched for associations with cell adhesion, actin cytoskeleton, wound healing and hypoxia response factors. Genes upregulated by EWS-FLI1 were enriched for associations to DNA replication, DNA repair, cell cycle, and chromatin remodeling factors. The loss of EWSR1 in A673 had fewer significant associations to cell functions. Genes downregulated by the EWSR1 knockdown included regulators of cell death and oxidative stress response factors, and those upregulated included mitochondrial proteins and lipid metabolism factors (**Supplemental Table 3-B**). The EWSR1 knockdown in HeLa cells yielded almost no associations in common with A673. However, specific associations could be identified for 206 genes affected in all EWS-FLI1 knockdown datasets for A673 and in our knockdown in A673 by siEWSR1 (**Figure 1E**, top). Of these genes, those with reduced transcript levels following the FLI1 knockdown or by siEWSR1 (n = 160) were enriched for collagen proteins, cell adhesion, and cell migration factors (**Figure 1E**, bottom). Chromatin binding proteins were enriched among the 46 genes upregulated across all the knockdown studies (**Supplemental Table 3-C**, and **3-D**). We found this analysis to suggest that EWSR1 may be a general and non-specific regulator of transcription but for cells expressing EWS-FLI1, genes associated with specific cellular functions became the targets for regulation by both proteins.

**EWSR1 is required for anchorage-independent growth in Ewing sarcoma.**

The loss of EWS-FLI1 can block anchorage-independent cell growth for Ewing sarcoma cell lines in soft agar colony formation assays (Smith et al. 2006; Chaturvedi et al. 2012). We hypothesized that an interaction between EWS-FLI1 and EWSR1 that was functional and significant to Ewing sarcoma biology may be reflected by changes to the tumorigenic capacity of cells in response to the knockdown of either protein.

We performed soft agar assays for A673 cells after EWSR1 or EWS-FLI1 knockdown. The knockdown of each protein was confirmed to be efficient and specific by western blot analysis (**Figure 2A**). We monitored cell growth and observed no change in the cell counts up to 4 days after each knockdown or the control siSCR treatment (**Supplemental Figure S2A**). Transfected A673 cells seeded on soft agar were grown for 3 to 4 weeks. The knockdown of EWS-FLI1 resulted in 60% fewer colonies relative to siSCR controls (n = 3, $p = 0.04$, Student's t-test, **Figure 2B**). Cells with the EWSR1 knockdown yielded 90% fewer colonies, revealing a dependency on EWSR1 for growth on soft agar (n = 3, $p = 0.004$, Student's *t*-test). We repeated the soft agar assays using SKNMC cells. By western blot analysis, the reduction of EWS-FLI1 or EWSR1 protein was found to be similar for knockdowns in SKNMC and A673 cells (**Supplemental Figure S2B**). In SKNMC cells, the EWS-FLI1 knockdown resulted in 80% fewer colonies and 90% fewer colonies for the EWSR1 knockdown (**Supplemental Figure S2C**). These results suggested that the loss of EWSR1 or EWS-FLI1 led to a similar loss in tumorigenic capacity for Ewing sarcoma cells. The EWSR1 knockdown might not be expected to affect tumorigenic capacity since the shRNA knockdown of EWSR1 found few effects on EWS-FLI1 target genes (Sankar et al. 2013). Conversely, the effects that siEWSR1 produced for EWS-FLI1 target genes would raise the expectation that either knockdown can yield the same reduction in cell growth we have observed in soft agar assays.

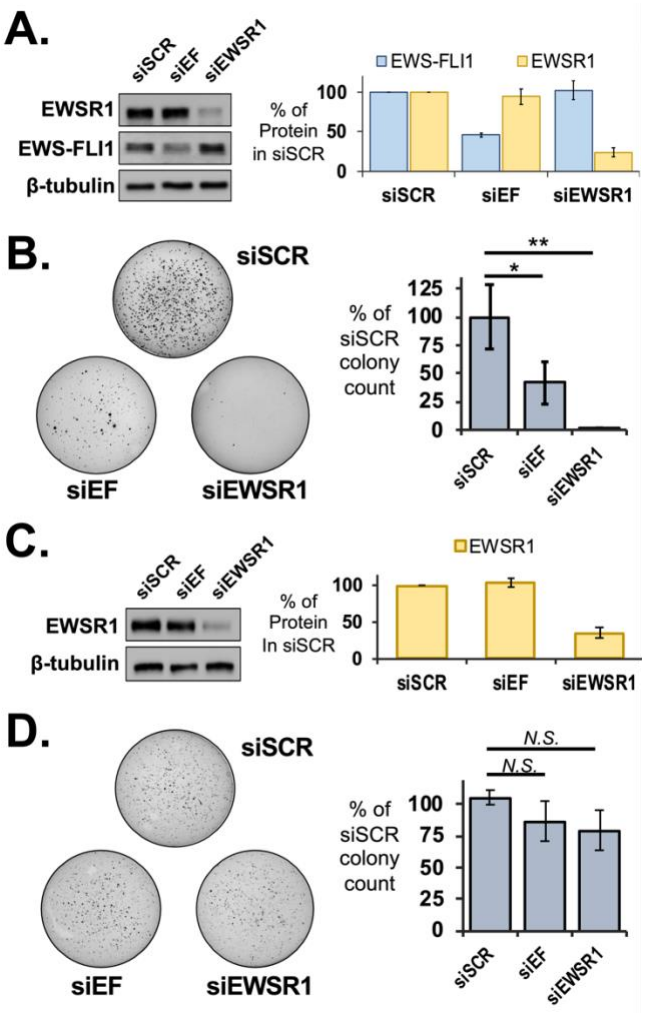


**Figure 2. Loss of EWSR1 inhibits anchorage-independent growth in Ewing sarcoma cells.** (**A**) Left, western assays reveal knockdown for EWSR1 or EWS-FLI1 in A673 cells for treatment with siSCR, siEF, or siEWSR1. Right, averaged levels of protein were determined by densitometry relative to siSCR treatments (n = 3). (**B**) Left, soft agar assays were performed with A673 cells treated with siSCR, siEF, or siEWSR1. Right, colonies were counted to reveal reductions in averaged values relative to siSCR treatment (n = 3). (**C**) Left, western assays reveal knockdown for EWSR1 or EWS-FLI1 in HEK293T/17 cells for treatment with siSCR, siEF, or siEWSR1. Right, averaged levels of protein were determined by densitometry relative to siSCR treatments (n = 4). (**D**) Left, soft agar assays were performed for HEK293T/17 cells treated with siSCR, siEF, or siEWSR1. Right, colonies were counted to reveal no change in averaged values relative to siSCR treatment (n = 4). All error bars represent standard

deviation. Student's *t*-test was calculated assuming equal variances: ** $p < 0.01$; * $p < 0.05$; n.s., not significant ($p > 0.05$).

The loss in colony growth after an EWSR1 knockdown in A673 cells could be interpreted as unrelated to EWS-FLI1 if a cell line without the fusion protein saw the same result. We chose a non-Ewing cell line, HEK293T/17 cells, to test the effects for the EWSR1 knockdown in a background without EWS-FLI1 or detectable FLI1 protein. Transfection with siEWSR1 effectively diminished EWSR1 protein but transfection with siEF had no effect (**Figure 2C**). HEK293T/17 cells treated with siEWSR1, siEF, or the siSCR control produced no difference in colony numbers on soft agar (n = 4, $p > 0.05$, Student's *t*-test, **Figure 2D**). This result left the possibility that EWS-FLI1 may impose a new role on EWSR1 in controlling cell phenotypes related to tumorgenicity.

Observing that an EWSR1 knockdown did not affect HEK293T/17 growth on soft agar, we asked whether the fusion protein could recreate the sensitivity to the loss of EWSR1 observed in Ewing sarcoma cells. We expressed V5-tagged EWS-FLI1 protein in HEK293T/17 cells (**Supplemental Figure S3A**). The expression of the fusion protein from a transfected plasmid did not inhibit growth of HEK293T/17 in the soft agar assay compared to an empty plasmid (**Figure 3A**). However, the knockdown of EWSR1 in HEK293T/17 cells expressing the fusion protein yielded 60% fewer colonies compared with the siSCR-treated control (n = 6, $p < 0.001$, Student's *t*-test, **Figure 3B**). The LC-domain shared by EWS-FLI1 and EWSR1 mediates homotypic interactions and binding to each other in cells (Chong et al. 2018; Gorthi et al. 2018; Boulay et al. 2017; Spahn et al. 2002). We confirmed this for V5-EWS-FLI1 expressed in these HEK293T/17 cells using a co-immunoprecipitation (co-IP) assay. With an EWSR1 specific antibody (B-1), we found by western assay V5-EWS-FLI1 protein eluted with EWSR1 and not in the control samples for an IP with non-specific IgG (**Supplemental Figure S3B**). As noted by previous studies, we found co-IP experiments in A673 were inconsistent in recovering endogenous EWS-FLI1 enriched by an EWSR1 IP above controls (**Supplemental Figure S3C**) (Spahn et al. 2003). We likewise interpreted the result to be influenced by a lower abundance of endogenous EWS-FLI1, the weakness in binding for homotypic and heterotypic interactions, or both.

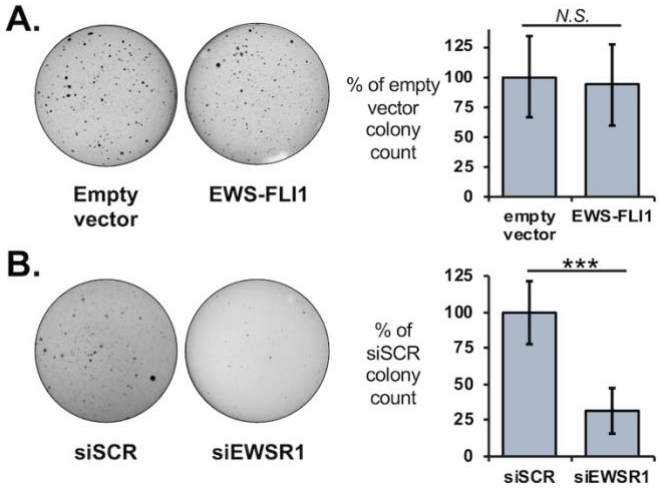


**Figure 3. EWS-FLI1 can alter effects on cell growth for an EWSR1 knockdown.** (**A**) Left, growth on soft agar was assessed for HEK293T/17 cells after transfection of empty plasmids or a plasmid expressing V5-EWS-FLI1. Right, colonies were counted to reveal no change in averaged values relative to siSCR treatment (n = 4). (**B**) Left, soft agar assays were performed with HEK293T/17 cells expressing V5-EWS-FLI1 and co-transfected with siSCR or siEWSR1 (n = 6). Right, colonies were counted to reveal a reduction in averaged values relative to siSCR treatment . Error bars represent standard deviation. Student's *t*-test was calculated for assuming equal variances: *** $p < 0.001$.

**EWSR1 and RNA Pol II associate with protein granules in cells**

The LC domain shared by FET proteins and fusion proteins driving Ewing sarcoma are capable of undergoing phase separation, a process that can form granules in cells (Kato et al. 2012; Kato and McKnight 2018; Lin et al. 2015). Consistent with the weak protein interactions for *in vitro* phase separation, granules in cells do not maintain their integrity after cell lysis (Wang et al. 2018; Qamar et al. 2018). Homotypic interactions for FET proteins have been confirmed in cells by previous studies (Spahn et al. 2003; Boulay et al. 2017; Kwon et al. 2013). To date, studies have not definitively established one of the several assemblies observed *in vitro* to be the predominant form in cells. These include (1) large multimer assemblies but of ordinary size for protein complexes in cells, (2) simple polymer or fiber-like assemblies, (3) large assemblies formed of relatively stable interactions described as hydrogels, or (4) condensates formed of weak interactions that give rise to liquid-like properties. We have previously developed

protocols that stabilize weak protein interactions for FET proteins with formaldehyde crosslinking (Thompson et al. 2018). With this approach, we characterized a granule formed by RNA Pol II transcription in cells. We now addressed whether EWSR1 associates with large macromolecular assemblies or condensates in cells.

We applied our SEC-based approach using lysates prepared from HEK293T/17 cells to separate large protein assemblies from ordinary molecular complexes and quantify amounts of EWSR1 and RNA Pol II in each fraction (Thompson et al. 2018). Important steps to the interpretation of our analysis by crosslinking include that all samples were subjected to sonication and nuclease treatment to minimize detection of assemblies tethered by nucleic acids rather than direct protein-protein interactions. Analysis using dynamic light scattering (DLS) indicated that SEC with a CL-2B column could separate particles from 14 nm to 150 nm in diameter (**Figure 4A**) (Thompson et al. 2018). The expected size of RNA Pol II is 25 nm at its longest axis. Particles of this size were observed at a 20 mL elution volume (**Figure 4A**, grey dashed line). UV absorption signals were maximal at >20 mL elution volumes, indicating most protein complexes or monomers were < 25 nm in diameter (n = 3, **Supplemental Figure S4A**). Lysates of crosslinked cells were prepared using buffers containing 6 M urea to prevent non-specific interactions not crosslinked in the cell. The UV trace for crosslinked samples did not differ appreciably from those with no crosslinking, indicating most proteins were not crosslinked in large assemblies (n = 3, **Supplemental Figure 4B**).

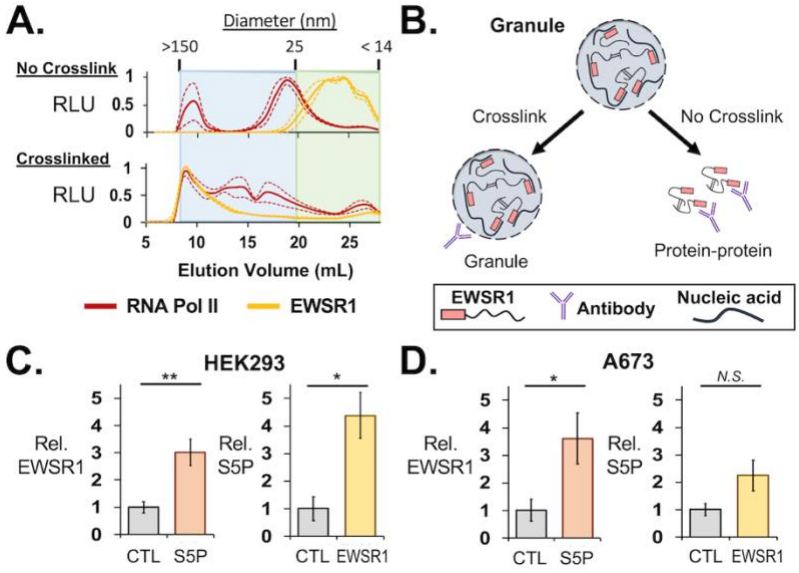


**Figure 4. EWSR1 and RNA Pol II are assembled in large protein assemblies.** (**A**) Total protein from HEK293T/17 cell lysates was analyzed by SEC to separate proteins, complexes, or assemblies by size. The averaged

ELISA signals are shown normalized to their maximum values for EWSR1 (C-9 antibody), yellow, or RNA Pol II (CTD4H8 antibody), red, as measured by ELISA. For samples from cells not crosslinked, top, RNA Pol II signals were highest in fractions eluting just before 20 mL, corresponding to particles of 25 nm in size. EWSR1 eluted after 20 mL or as a particle < 25 nm in size. For crosslinked samples, bottom, the elution of EWSR1 and RNA Pol II shifted to early fractions with particles measured to be up to 150 nm in diameter. Dashed lines represent standard error about the mean (n = 3). (**B**) IP assays using cells without crosslinking enrich for ordinary and stable molecular complexes. Those using crosslinked cells can recover large molecular assemblies that form by weak protein interactions. (**C**) Left, ELISA assays detected EWSR1 eluted from crosslinked IP assays of phosphorylated (S5P) RNA Pol II (Abcam, ab5131) in HEK293T/17 cells (n = 3). Right, S5P RNA Pol II was detected for crosslinked IP of EWSR1 (B-1 antibody) (n = 3). (**D**) Left, ELISA assays in A673 cells also detected EWSR1 eluted with S5P RNA Pol II. Right, S5P RNA Pol II was detected in crosslinked IP assays of EWSR1 (n = 3). All error bars represent standard error about the mean. AU = absorbance units. RLU = relative luminescence units. Student's *t*-test was calculated assuming equal variances: ** $p < 0.01$; * $p < 0.05$; *n.s.*, not significant ($p > 0.05$).

We performed ELISA assays on the SEC fractions collected using antibodies for RNA Pol II (CTD4H8) and EWSR1 (C-9) . As we have previously reported, RNA Pol II eluted just before and near 20 mL, suggesting a particle somewhat larger than 25 nm in diameter (**Figure 4A**, top). The sum of signals quantitated by ELISA indicated that 25% of RNA Pol II was present in particles >50 nm in diameter for cells not treated with formaldehyde. SEC of lysates prepared from crosslinked cells indicated 54% of the total RNA Pol II detected eluted at volumes < 15 mL, for which particle were >50 nm in diameter (**Figure 4A**). EWSR1 was observed to elute in volumes >20 mL, indicating either small complexes or monomers were present in lysates not crosslinked. In crosslinked cells, 71% of the total EWSR1 detected was found in early fractions for particles of at least 50 nm in diameter. We have previously determined by DLS measurements, the first SEC fraction yielded a signal of 150 nm as the diameter of particles at this void volume of the column. Lysates were passed through a 0.45 μm filter before SEC and by TEM, the void fraction was observed to contain particles of up to 300 nm (Thompson et al. 2018). This suggests that particles eluting early may be bigger than 150 nm but are unlikely to be much bigger than 0.3 μm.

We tested whether interactions between EWSR1 and RNA Pol II were crosslinked in HEK293T/17 cells. This approach allows robust detection for weak interactions that would be rarely observed in standard IP protocols, and can be treated with strong detergents to prevent detection of non-specific interactions by these aggregation prone disordered proteins (**Figure 4B**). For IP experiments in HEK293T/17 cells, an antibody specific for the serine-5 phosphorylated (S5P) form of RNA Pol II (Abcam, ab5131) and was found to yield more efficient protein in the IP elution. An antibody specific for the EWSR1 C-terminus (B-1) was used for IP experiments. Significant enrichment for EWSR1 eluting with the polymerase was observed in ELISA assays, relative to a negative control using protein G beads (n = 3, $p$ = 0.009, Student's *t*-test, **Figure 4C**, left). An IP for EWSR1 similarly found enrichment for S5P RNA Pol II (n = 3, $p$ = 0.02, Student's *t*-test, **Figure 4C**, right). We repeated the IP assays using crosslinked A673 cells, which confirmed crosslinking of interaction of S5P RNA Pol II with an EWSR1 IP (n = 3, $p$ = 0.04, Student's *t*-test, **Figure 4D**). The interaction with EWSR1 in A673 cells was enriched in an S5P RNA Pol II IP but without reaching significance (n = 3, $p > 0.05$, Student's *t*-test).

**EWS-FLI1 is found in a protein granule in cells**

We lastly investigated the interactions and cellular assemblies occupied by EWS-FLI1. When observed *in vitro*, higher order assemblies for FET and other LC domain proteins have been observed in a number of alternative structures that vary in appearance and physical characteristics (Qamar et al. 2018; Lin et al. 2015; Kwon et al. 2013; Schwartz et al. 2013). Under electron microscopy, ordinary protein complexes are visibly distinct from amyloid-like fibers, amorphous aggregates, or the rounded structures of the phase separation process that can form a granule in cells. We now sought to characterize EWS-FLI1 associations with RNA Pol II protein assemblies and observe whether EWS-FLI1 or RNA Pol II assemblies contrasted in their physical characteristics that might indicate similar or wholly independent assembly processes.

We tested whether EWS-FLI1 was crosslinked with assemblies of EWSR1 and RNA Pol II. Analogous to the approach used for analysis by SEC, crosslinked cells were lysed in the presence of 1% SDS to ensure interactions detected were due to crosslinks made in the cell rather than non-specific or aggregation after lysis. Steps were included to cleave interactions tethered by nucleic acids to enrich for protein-protein crosslinked interactions. HEK293T/17 cells were transfected with V5-tagged EWS-FLI1 for use in co-IP assays. Antibodies binding the C-

terminal portions of either EWSR1 (B-1) or EWS-FLI1 (Abcam, ab15289) allowed specificity for the assay in A673 cells. For RNA Pol II, the CTD4H8 antibody from mouse was used to avoid interference with EWS-FLI1 antibody signals. By ELISA, EWS-FLI1 was found highly enriched in EWSR1 IP samples compared with negative protein G bead controls (n = 3, $p = 0.01$, Student's *t*-test, **Figure 5A**). EWS-FLI1 was likewise enriched in RNA Pol II IP experiments compared with negative controls (n = 3, $p = 0.03$, Student's *t*-test, **Figure 5A**). EWSR1 (C-9) and RNA Pol II (CTD4H8) was also found in the IP of EWS-FLI1 expressed in HEK293T/17 cells (**Supplemental Figure S5A** and **S5B**).

We confirmed that interactions stabilized by crosslinking were dependent on the key tyrosine residues of the LC domain by expressing an V5-tagged EWS-FLI1 protein with 37 tyrosine residues in the [S/G]Y[S/G] motif replaced by serine (YS37, *provided by the lab of M. Rivera*) (Boulay et al. 2017). We transfected this construct in HEK293T/17 cells and found expression comparable to that of wild-type V5-EWS-FLI1 (**Supplemental Figure S5C** and **S5D**). For crosslinked HEK293T/17 cells, EWSR1 or RNA Pol II did not pulldown the YS37 fusion protein (n = 3, $p > 0.05$, Student's *t*-test, **Figure 5B**). The reciprocal IP of YS37 also did not find enrichment of EWSR1 or RNA Pol II (**Supplemental Figure S5E** and **S5F**). This result suggested that stabilizing protein interactions by crosslinking could not provide evidence of an EWSR1 or RNA Pol II interaction with an EWS-FLI1 unable to homo-oligomerize through the LC domain. In contrast to our result without crosslinking, we could observe EWSR1 and RNA Pol II in the IP of endogenous EWS-FLI1 from crosslinked A673 cells. Similarly, EWS-FLI1 eluted with EWSR1 or RNA Pol II at significant levels over negative controls when stabilized by crosslinking (n = 4, $p < 0.05$, Student's *t*-test, **Figure 5C**).

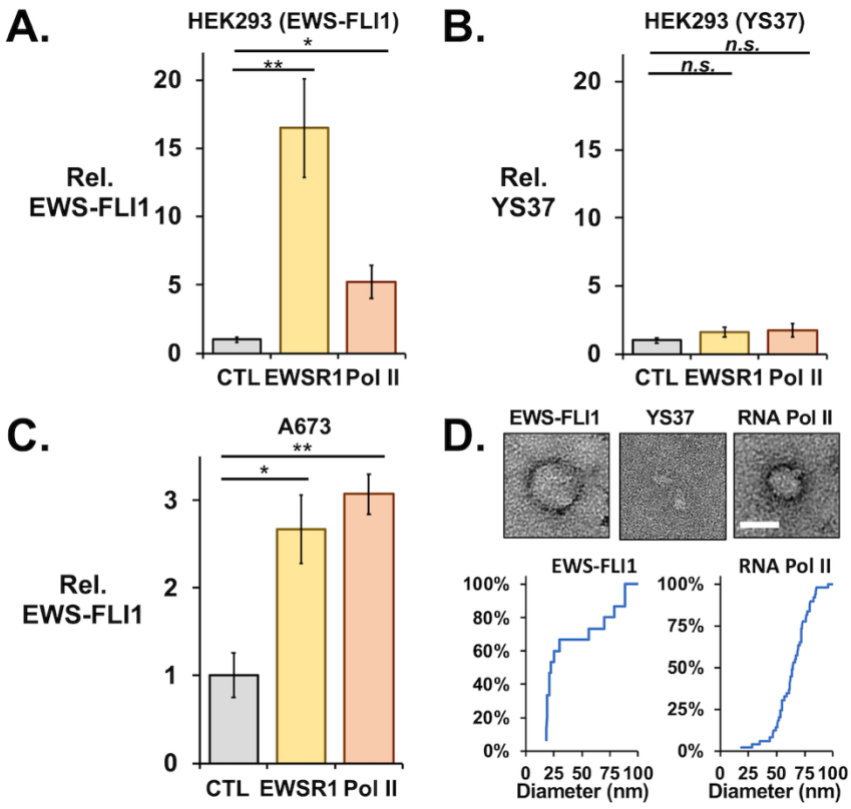


**Figure 5. EWS-FLI1 and RNA Pol II coimmunoprecipitate in crosslinked protein granules.** ELISA assays using an antibody to FLI1 measured interactions with FLI1-fusion proteins recovered by co-IP assays from crosslinked cells. The IP of EWSR1 (B-1) or RNA Pol II (CTD4H8) recovered V5-EWS-FLI1 (**A**) but not YS37 (**B**) protein expressed in HEK293T/17 cells by plasmid transfections (n = 3 each). (**C**) Crosslinked IP assays of EWSR1 and RNA Pol II also recovered endogenous EWS-FLI1 from A673 cells (n = 4). (**D**) Transmission electron microscopy detected protein particles recovered from crosslinked HEK293T/17 cells by IP of EWS-FLI1 (anti-FLI1 antibody, left) and RNA Pol II (CTD4H8, left), but not of YS37 (anti-FLI1 antibody, center). Scale bar inset represents 50 nm. Cumulative plots show diameters for particles imaged in IP samples for EWS-FLI1 (n = 24) or RNA Pol II (n = 77). All error bars represent standard error about the mean. Student's *t*-test was calculated assuming equal variances: ** $p < 0.01$; * $p < 0.05$; n.s., not significant ($p > 0.05$).

We have previously reported imaging by transmission electron microscopy (TEM) of crosslinked particles associating with RNA Pol II in cells (Thompson et al. 2018). These particles typically appeared round and 50 nm in diameter but could measure up to 270 nm. Their circular shapes could indicate a sphere when in solution, as

expected for particles of weak interactions, including liquid-like condensates. We investigated whether the crosslinked assemblies in HEK293T/17 cells shared these properties. By negative-stained TEM, an RNA Pol II IP from crosslinked HEK293T/17 cells yielded round particles up to 95 nm in diameter. Particles sizes averaged 64 ± 15 nm in diameter (n = 77, **Figure 5D**). We imaged samples treated with proteinase K, which eliminated the round particles observed and indicated they were comprised of protein (**Supplemental Figure S6**).

For crosslinked HEK293T/17 cells that expressed V5-EWS-FLI1, we imaged by TEM particles that were also round in shape and varied in size, with an average diameter of 42 ± 27 nm (n = 24, **Figure 5D,** left). To test whether the role of the LC domain, we repeated the assay and TEM imaging using crosslinked HEK293T/17 cells that expressed the YS37 variant of EWS-FLI1. The YS37 IP did not recover round particles visible to TEM (**Figure 5D**). We concluded that protein assemblies associated with EWS-FLI1 were similar shape and comparable size to those observed for RNA Pol II. Their assembly depended on the oligomerization domain of EWS-FLI1. These physical properties observed of particles associated with EWS-FLI1 or RNA Pol II in cells appear consistent with condensates and did not indicate substantial differences in their structural makeup or suggest they had formed by unrelated molecular processes.

## DISCUSSION

The N-terminal domains of FET proteins allow them to oligomerize with disordered domains of similar low complexity and amino acid composition (Murray et al. 2017; Schwartz et al. 2015). We compared the roles of EWSR1 and EWS-FLI1 to control gene expression and found that EWS-FLI1 and EWSR1 regulate transcription for hundreds of identical gene targets. EWSR1 and the fusion protein each affect the signature property of transformation, anchorage-independent cell growth. The same deficiency in growth on soft agar indicates a functional interaction but without distinguishing whether this reflects protein-protein binding. The same assay for a non-Ewing cell line is not affected by the EWSR1 knockdown, but the effect was reproduced when the fusion protein was introduced. This result indicates that interactions between EWS-FLI1 and EWSR1 are significant enough to alter the cellular function of these proteins.

We investigated the weak interactions of EWSR1, EWS-FLI1, and RNA Pol II after they were stabilized by formaldehyde crosslinking. Crosslinking allowed their associations with large protein assemblies to be observed in

analysis by SEC or IP assays. Even when stabilized by crosslinking, EWS-FLI1 binding to EWSR1 or RNA Pol II required its tyrosine-rich LC domain. Inspection by TEM of particles associated with RNA Pol II or EWS-FLI1 found round structures of comparable size and appearance and resembling a cell granule formed through weak protein interactions. Visual inspection of EWS-FLI1 assemblies finds greater consistency with forms adopted by liquid-like condensates, rather than alternative structures that can also be observed in *in vitro* studies, such as fibers or amorphous aggregates (Kwon et al. 2013; Chong et al. 2018). The association of EWS-FLI1 with the large assemblies observed in TEM offers a model that may account for the ability of EWS-FLI1 to bind with its large network of protein partners associated with the control of gene expression (Gorthi et al. 2018; Boulay et al. 2017; Sankar and Lessnick 2011).

EWS-FLI1 target genes were found to be regulated by EWSR1 with a greater frequency than expected (Sankar et al. 2013). One significant difference between this and previous studies is the method of knockdown. The knockdown in this study used siRNA transfection producing a relatively brief exposure for cells to the loss of protein. A stable knockdown by lentiviral shRNA vector requires cells to be cultured for at least 2 weeks in the absence of the protein. Several arguments indicate that observed EWSR1 knockdown effects in this study are not off target. Effects of the EWSR1 or EWS-FLI1 knockdowns do not overlap randomly (**Figure 1E**). Our EWSR1 knockdown affects established EWS-FLI1 targets identified by multiple studies, including those repressed and up-regulated (Miller et al. 2020; Selvanathan et al. 2015; Stoll et al. 2013; Bilke et al. 2013; Smith et al. 2006). Enrichment of the same GO associations can be seen among genes affected by the loss of EWSR1 or EWS-FLI1 in A673 cells. Few genes affected by EWSR1 in A673 cells were the same found in an siRNA knockdown in HeLa cells. Among those affected by EWSR1 in both cell lines were also targets of EWS-FLI1 (**Figure 1D**). Excluding genes targeted by EWS-FLI1, our analysis does not indicate EWSR1 specifically targets genes based a role they play in the cell or signal pathways. Data provided by the siRNA knockdown can indicate that EWSR1 participates in a function that is generally important to EWS-FLI1 activity. The comparison of this data to those from a stable EWSR1 knockdown suggests that EWSR1 is not irreplaceable for the function it serves. A model for EWSR1 to contribute to forming structures required for EWS-FLI1 activity may allow for a substitute with similar abilities to replace EWSR1 when the protein was knocked down or if it became lost during a tumor's development.

In addition to the large number of genes affected by both EWSR1 and EWS-FLI1, the capacity for anchorage-independent growth was affected by both proteins, which extends the functions in common for the fusion and wild-type proteins to include cellular functions (**Figure 2B**). A role for EWSR1 in this aspect of cell growth is not typical of transformed cells, as demonstrated in HEK293T/17 cells (**Figure 2D**). The similar effects in soft agar assays are consistent with the similarity in changes to gene expression observed by our RNA-seq analysis. Those genes unaffected by EWSR1 may potentially rank lower in significance to growth in the soft agar assay. However, expression of EWS-FLI1 from a transfected plasmid was sufficient to reproduce the effect of EWSR1 on anchorage independent growth (**Figure 3B**). This result suggests EWS-FLI1 can modify EWSR1 activity or vis versa (Abraham et al. 2020; Gorthi et al. 2018). Future studies may find that these two approaches have potential to reveal still more understanding of the relationship of EWSR1 to EWS-FLI1. Cells that thrive without EWSR1 may possess or acquire epigenetic markers able to indicate their mechanism for adaption, which by comparison can reveal more specific details of the function offered by EWSR1 and critical to EWS-FLI1 activities that lead to tumorigenesis.

The mechanisms by which FET proteins and their fusion products interact with RNA Pol II have the potential to influence paradigms for transcription regulation in higher eukaryotes (Abraham et al. 2020; Zamudio et al. 2019; Chong et al. 2018; Thompson et al. 2018). FET proteins bind the polymerase *in vitro* at part of a higher order assembly (Schwartz et al. 2013; Kwon et al. 2013). Assemblies of FET proteins or their fusions vary by appearance when formed *in vitro* and each form, if observed in cells, place architectural constraints for interactions made with the transcription machinery (McSwiggen et al. 2019a; Thompson et al. 2018; Murray et al. 2017; Schwartz et al. 2013). Tyrosine residues in the LC domains appear essential to every type of homotypic or heterotypic interaction for EWS-FLI1 or EWSR1 studied in cells, including binding to DNA microsatellites (Johnson et al. 2017; Boulay et al. 2017; Kwon et al. 2013). Both proteins precipitate with biotinylated isoxazole, b-isox, which was once interpreted to indicate amyloid-like fiber structures (Murray et al. 2017; Kato et al. 2012). Fibrous assemblies of FET and FET fusion proteins observed *in vitro* are comparable in size to EWSR1 or RNA Pol II assemblies we observe in SEC analysis (**Figure 4A**). Liquid-like condensates formed *in vitro* favor minimally energetic round shapes or spheres in suspension (Springhower et al. 2020; McSwiggen et al. 2019b; Lin et al. 2015; Molliex et al. 2015). Observations of EWS-FLI1 and RNA Pol II particles from cells found only rounded forms and neither fibers nor evidence for a fibrillar structure within these particles (**Figure 5D**). The vacuum required for TEM imaging can

account for the flattened appearance of EWS-FLI1 or RNA Pol II particles (Thompson et al. 2018). Water has been noted to comprise much of the volume for *in vitro* formed condensates of FET proteins. These observations noted for the EWS-FLI1 assemblies are consistent with structures formed by weak interactions that comprise either cellular condensates or granules.

The inclusion of fusion proteins driving Ewing sarcoma into granules or condensates can raise exciting new questions to be explored. How many interactors of EWS-FLI1 possess oligomerization properties similar to EWSR1? Protein playing a structural role in EWS-FLI1 assemblies may add new functionality or modify the structural role of other protein components. Second, are more hnRNP proteins and RNA processing machineries recruited to sites in DNA occupied by EWS-FLI1 and related fusion proteins? If true, at least three possibilities can be explored: RNA polymerase can be recruited by RNA processing machinery to initiate gene transcription; the fusion protein can repress transcription by directing crucial RNA processing machinery elsewhere; and, the localization of RNA processing machinery contributes to reprogram transcription and driving tumorigenesis. Last, RNA-binding proteins that bind RNA promiscuously are recruited by the fusion protein, what RNA transcripts associate with the assemblies and what role can they serve? The answer to these questions is likely to depend on knowledge of how many assemblies or granules can incorporate EWS-FLI1, including any that may be unbound by DNA. The diversity of affects that EWS-FLI1 has on gene expression may become easier to rationalize if these effects could be separated based on which type of EWS-FLI1 assembly was involved.

## MATERIALS AND METHODS

### Cell Culture

Cell lines were obtained from American Type Culture Collection. A673 (ATCC-CRL-1598) and SK-N-MC (ATCC-HTB-10) cells were grown in Dulbecco's modified Eagle Medium (DMEM, Thermo Fisher) supplemented with 10% fetal bovine serum (FBS). HEK293T/17 (ATCC-CRL-11268) cells were grown in DMEM supplemented with 5% FBS. All cell lines were cultured at 37°C and 5% $CO_2$.

### Plasmid and siRNA Transfections

Sequences for siRNAs used are provided in **Supplemental Table 1** and were purchased commercially (Sigma-Aldrich). Oligonucleotides were annealed to form siRNA duplexes by heating to 95 ºC in PBS and cooled at room temperature. The plasmids used, pLV-V5-EWS-FLI1 and pLV-V5-EWS(YS37)-FLI1, were a gift from the M. Rivera lab (Harvard Medical School, Charlestown MA). A673 cells ($5.0 \times 10^5$) in 6-well dishes were reverse transfected with siRNA (50 nM) using Lipofectamine™ RNAiMAX (Invitrogen, cat. no.13778075) according to manufacturer's instructions. HEK293T/17 and SK-N-MC cells ($4.0 \times 10^5$) were seeded in 6-well dishes and transfected with siRNA (50 nM) after 24 hours using the TransIT-X2 lipid reagent (Mirus Bio cat. no. MIR6000) or RNAiMAX™. Cells were harvested 48 to 72 hours after siRNA transfections. HEK293T/17 cells grown to 80% confluency for transfection with plasmid (2 μg) using the TransIT-X2 lipid reagent and according to manufacturer's instructions. Cells transfected with plasmids or plasmid with siRNA were harvested 48 to 96 hours post-transfection.

Knockdown efficiency was assessed for siRNAs screened for use in this study by real time PCR using a StepOne Plus Real-Time PCR System (Applied Biosystems). Total cell RNA was harvested using Trizol™ (Life Technologies) and cDNA synthesized using the High Capacity cDNA Reverse Transcription Kit (Life Technologies), which uses random primers. Real-time PCR was performed with the TaqMan® Universal PCR Master Mix (Life Technologies). Commercially designed primers (Taqman gene expression assay, Thermo Fisher) were purchased for FLI1 (Hs04334143_m1), EWSR1 (Hs01580532_g1), and the Human GAPD (GAPDH) Endogenous control. Relative change in cDNA was calculated using the $\Delta\Delta C_T$ method and normalized to the GAPDH control.

**Western Blot Analysis**

Protein lysate concentrations were quantified using the bicinchoninic (BCA) protein assay (ThermoFisher, cat. no. 23227). Protein samples of 5 to 10 μg were loaded onto 7.5% SDS-PAGE gels. Blots were transferred at 500 mA, blocked in 5% nonfat dried milk in Tris-buffered saline-Tween (TBS-T), and incubated overnight with primary antibody at 4°C. Blots were washed in TBS-T, incubated in secondary antibody for 1 hour at room temperature, washed again in TBS-T, and imaged after the addition of SuperSignal™ West Pico PLUS Chemiluminescent substrate (ThermoFisher, cat. no. 34578). Antibodies used in western blots were anti-EWSR1 (clone B-1, Santa Cruz Biotechnology, cat. no. 398318), anti-FLI1 (Abcam, cat. no. 15289), anti-RNA Pol II (clone CTD4H8, EMD

Millipore, cat. no. 05-623), anti-RNA Pol II CTD phospho S5 (Abcam, cat. no. 5131), and anti-V5 (Abcam, cat. no. 27671); secondary antibodies used were donkey anti-mouse IgG horseradish peroxidase (HRP) (Jackson ImmunoResearch, cat. no. 715-035-15) and donkey anti-rabbit IgG HRP (Jackson ImmunoResearch, cat. no. 711-035-152).

**RNA Sequencing**

A673 cells were transfected with 50 nM siRNA as described above. Cells were collected 72 hours post-transfection and total RNA was extracted using TRIzol reagent (ThermoFisher, cat. no. 15596026). RNA (1 μg) was prepared for sequencing using NEBNext Poly(A) mRNA Magnetic Isolation Module (New England Biolabs, cat. no. E7490) to generate sequencing libraries according to the manufacturer's instructions.

RNA samples were sequenced with an Illumina HiSeq2500 to yield between 20M to 32M 100 bp paired end reads (N = 2 per treatment). Changes in transcript abundance were analyzed according the workflow for the Cufflinks suite of tools using TopHat v2.1.1 (https://ccb.jhu.edu/software/tophat/index.shtml) and Cufflinks v2.2.1 (http://cole-trapnell-lab.github.io/cufflinks/). Alignments were made to the hg38 REFSEQ annotated transcripts. The program Cuffcompare was used to assemble a common transcriptome for comparison across this and previously published studies (Trapnell et al. 2012). Bam files can be viewed through a genome browser by copying the html links provided here (SCR1, SCR2, siEF1, siEF2, siEWSR1-1, siEWSR1-2, siE-EF1, and siE-EF2). Datasets generated by this study are publicly available under GEO Accession no. GSE154944. Alignment statistics for all RNA-seq data analyzed in this study are provide in **Supplemental Table 1**. Fold changes for the top 10k gene transcripts used for this study are found in **Supplemental Table 2**. Network analysis was performed using Cytoscape v3.7.2 and the BiNGO app using default settings and the ontology files: GO_Cellular_Component, GO_Molecular_Function, and GO_Biological_Process (Excoffier et al. 2017; Shannon et al. 2003). A full list of GO associations found by network analysis is found in **Supplemental Table 3**.

**Soft Agar Colony Formation Assay**

A673, SK-N-MC, and HEK293T/17 cells transfected with 50 nM siRNA were harvested at 24 hours post-transfection. HEK293T/17 cells transfected with 50 nM siRNA and 2 μg of plasmid DNA were harvested 24 hours

post-transfection. A673 and SK-N-MC cells were seeded at density of $1.0 \times 10^5$ cells. Cells were resuspended in 0.35% agarose in growth medium and plated onto a bed of solidified 0.6% agarose in growth media. HEK293T/17 cells were seeded at a density of 20k to 30k cells. Cells were resuspended in 0.4% agarose in growth medium onto a bed of solidified 0.6% agarose in growth media. A673 and SK-N-MC cells were grown at 37°C and 5% $CO_2$ for 3 to 4 weeks, imaged, and then colonies were counted using ImageJ software. HEK293T/17 cells were grown at 37°C and 5% $CO_2$ for 1 to 2 weeks, imaged, and then colonies were counted. Colonies with stained with 0.05% methylene blue.

**Cell Growth Assay**

A673 cells were reverse transfected at a density of $4.0 \times 10^5$ cells in 6-well dishes. Cells were collected by trypsinization and counted on a hemocytometer at 24, 48, 72, and 96-hour time points post-transfection.

**Co-Immunoprecipitation Assay**

Co-immunoprecipitation assays (co-IP) performed with uncrosslinked cells were grown to confluency in 6-well plates. Cells were harvested and lysed in co-IP lysis/wash buffer (25 mM Tris-HCl pH 7.4, 200 mM NaCl, 1 mM EDTA, 0.5% NP40, 5% glycerol). Protein A/G agarose beads (EMD Millipore, cat. no. IP05) were incubated with primary antibody for 2 hours at 4°C before addition to cell lysate. Lysate was incubated with beads-antibody complex overnight with rotation at 4°C. Beads were washed 5 times in co-IP lysis/wash buffer, resuspended in Novex NuPage™ Sample Loading Buffer (Fisher Scientific, cat. no. np0008) with 5 mM dithiothreitol (DTT) and boiled for 5 minutes at 95°C. Beads were then centrifuged at 8000 rpm and eluted protein removed with the supernatant and detected by western blot.

For crosslinked co-IP assays, cells were harvested from confluent 150-mm dishes. Cells were crosslinked using 1% formaldehyde for 15 minutes and then quenched with glycine (125 mM). Cells were washed in phosphate-buffered saline (PBS) and lysed in Buffer B (1% SDS, 10 mM EDTA, 50 mM Tris-HCl pH 8.0) supplemented with protease inhibitors. Lysate was sonicated using a Bioruptor Pico (Diagenode) for 30 minutes and then centrifuged at maximum speed (20000×*g*) for 30 minutes at 4°C. Crosslinked lysate was diluted 10-fold in IP lysis buffer (0.01% SDS, 1.1% Triton-X, 1.2 mM EDTA, 16.7 mM Tris-HCl pH 8.0, 167 mM NaCl) treated with protease inhibitors

(Sigma-Aldrich, cat. no. P8340) and benzonase (Millipore-Sigma, cat. no. 70746). Lysate was then incubated with rotation overnight with primary antibody at 4°C. Antibody-bound complexes were immunoprecipitated with Novex DYNAL Dynabeads Protein G (Invitrogen, cat. no. 10-003-D) or protein A/G agarose beads (EMD Millipore, cat. no. IP05) for 2 hours at room temperature. Beads were washed 5 times using IP lysis buffer and eluted in 3.6 M $MgCl_2$ and 20 mM 2-(*N*-morpholino)ethanesulfonic acid (MES, pH 6.5) for 30 minutes with agitation. IP samples were then assayed for proteins by ELISA.

IP experiments were performed with antibodies to EWSR1 (clone B-1, Santa Cruz Biotechnology, cat. no. 398318), FLI1 (Abcam, cat. no. 15289), RNA Pol II (clone CTD4H8, EMD Millipore, cat. no. 05-623), phospho S5 RNA Pol II (Abcam, cat. no. 5131), and V5 (Abcam, cat. no. 27671). Elutions were probed by western assay for uncrosslinked samples or by ELISA for crosslinked samples.

**Size Exclusion Chromatography**

The protocol for SEC of crosslinked lysates has been previously described (Thompson et al. 2018). For crosslinked lysates, cells were harvested from confluent 150-mm dishes. Cells were crosslinked in 1% formaldehyde for 15 minutes and then quenched in 125 mM glycine. Cells were harvested by scraping, washed in PBS, and resuspended in 5 to 10 volumes of Buffer C (400 mM NaCl, 20 mM HEPES pH 7.9, 5% glycerol, 0.75 mM $MgCl_2$, and 6 M urea). Lysates were sonicated using a Bioruptor Pico (Diagenode) for 30 minutes at 4°C, followed by centrifugation at maximum speed (20000×*g*) for 30 minutes at 4°C , then filtered through a Costar Spin-X 0.45 μm filter (VWR, cat. no. 8163). Lysate (1 to 2 mg) was injected onto the column. SEC was performed using a Sepharose CL-2B 10/300 column (Sigma-Aldrich, cat. no. CL2B300, 100 mL) injected with lysates from HEK293T/17 or A673 cells. Columns were run in Buffer B (100 mM NaCl, 20 mM HEPES pH 7.9, 0.2 mM EDTA, 5% glycerol, 6 M urea, and 0.5 mM DTT). SEC experiments were analyzed by ELISA as described below with antibodies to EWSR1 (clone C-9, Santa Cruz Biotechnology cat. no. sc-48404) and RNA Pol II (clone CTD4H8, EMD Millipore, cat. no. 05-623).

**ELISA**

ELISAs were performed in 96-well Greiner LUMITRAC-600 white plates (VWR, cat. no. 82050-724). ELISAs were performed as indirect ELISAs, in which protein samples from SEC or crosslinked IP assays were incubated in plates overnight at 4°C. Afterward, plates were washed 3 times in TBS-T, blocked for 2 hours at room temperature in 5% nonfat dried milk in TBS-T, washed 4 times in TBS-T and then incubated with primary antibody overnight at 4°C. After incubation with primary antibody, plates were washed 4 times in TBS-T and incubated with secondary antibody, goat anti-mouse IgG HRP (ThermoFisher cat. no. 31432) or goat anti-rabbit IgG HRP (ThermoFisher, Cat. #31462) for 1 hour at room temperature. Finally, plates were washed 4 times with TBS-T and proteins were detected by addition of SuperSignal™ ELISA Femto substrate (ThermoFisher cat. no. PI37074). Luminescence was read using a BMG POLARstar Omega plate reader or Biotek Neo2 microplate reader.

**Transmission Electron Microscopy**

TEM assays were performed for samples from co-IP assays using antibodies to RNA Pol II (CTD4H8) or FLI1 (Abcam, cat. no. 15289). Carbon Film 300 Mesh Copper grids (Electron Microscopy Sciences, cat. no. CF300-CU) were charged at 15 mA for 30 seconds. Crosslinked immunoprecipitation samples were spotted onto charged grids and stained with 0.75% uranyl formate. For proteinase K-treated samples, the samples were treated with 5 μg of proteinase K and incubated for 30 minutes at 37°C before being spotted onto grids and stained with 0.75% uranyl formate. Images were collected from a FEI Tecnai Spirit 120S or FEI Tecnai F20 transmission electron microscope. Diameters of particles observed were measured with ImageJ software (U. S. National Institutes of Health, Bethesda, Maryland, USA, https://imagej.nih.gov/ij/).

## Corresponding Author

Correspondence should be addressed to Jacob C. Schwartz at jcschwartz@arizona.edu.

## Author Contributions

N.S.A. designed and performed experiments, analyzed data, and interpreted results. L.M.H. contributed the design of siRNAs, performed the screening and optimization siRNA knockdown using real-time PCR and western assays, and contributed to multiple procedures involving recombinant DNA. N.S.A. wrote the first draft of the manuscript. J.C.S. contributed to analysis of RNA-seq data. N.S.A. and J.C.S. collaborated to write subsequent drafts. All authors have approved to the final version of the manuscript.

## Funding Sources and Acknowledgements

This work was supported by funding from the National Institutes of Health (R21CA238499) and the American Cancer Society (RSG-18-237-01-DMC) to J.C.S. Additional support was provided by National Institute of General Medicine (T32-GM008659) training grant awarded to N.S.A. Next-generation sequencing was performed by the University of Arizona Genetics Core, http://uagc.arizona.edu. Transmission election microscopy was performed with the Eyring Materials Center at Arizona State University, supported in part by NNCI-ECCS-1542160. Transmission Electron Microscopy was also performed through the University of Arizona Office of Research, Innovation, & Impact Imaging Cores. Research reported in this publication was also supported by the Office of the Director, National Institutes of Health of the National Institutes of Health, under award number S10OD013237.

## REFERENCES

Abraham KJ, Khosraviani N, Chan JNY, Gorthi A, Samman A, Zhao DY, Wang M, Bokros M, Vidya E, Ostrowski LA, et al. 2020. Nucleolar RNA polymerase II drives ribosome biogenesis. *Nature*.

Bilke S, Schwentner R, Yang F, Kauer M, Jug G, Walker RL, Davis S, Zhu YJ, Pineda M, Meltzer PS, et al. 2013. Oncogenic ETS fusions deregulate E2F3 target genes in Ewing sarcoma and prostate cancer. *Genome Res* **23**: 1797–1809. https://www.ncbi.nlm.nih.gov/pubmed/23940108.

Boulay G, Sandoval GJ, Riggi N, Iyer S, Buisson R, Naigles B, Awad ME, Rengarajan S, Volorio A, McBride MJ, et al. 2017. Cancer-Specific Retargeting of BAF Complexes by a Prion-like Domain. *Cell* **171**: 163-178.e19.

Chaturvedi A, Hoffman LM, Welm AL, Lessnick SL, Beckerle MC. 2012. The EWS/FLI Oncogene Drives Changes in Cellular Morphology, Adhesion, and Migration in Ewing Sarcoma. *Genes and Cancer* **3**: 102–116.

Chi B, O'Connell JD, Yamazaki T, Gangopadhyay J, Gygi SP, Reed R. 2018. Interactome analyses revealed that the U1 snRNP machinery overlaps extensively with the RNAP II machinery and contains multiple ALS/SMA-causative proteins. *Sci Rep* **8**: 8755. https://www.ncbi.nlm.nih.gov/pubmed/29884807.

Chong S, Dugast-Darzacq C, Liu Z, Dong P, Dailey GM, Cattoglio C, Heckert A, Banala S, Lavis L, Darzacq X, et al. 2018. Imaging dynamic and selective low-complexity domain interactions that control gene transcription. *Science (80- )* **361**.

Delattre O, Zucman J, Plougastel B, Desmaze C, Melot T, Peter M, Kovar H, Joubert I, De Jong P, Rouleau G, et al. 1992. Gene fusion with an ETS DNA-binding domain caused by chromosome translocation in human tumours. *Nature* **359**: 162–165.

Excoffier L, Gouy A, Daub JT, Shannon P, Markiel A, Ozier O, Baliga NS, Wang JT, Ramage D, Amin N, et al. 2017. Cytoscape: A Software Environment for Integrated Models of Biomolecular

Interaction Networks. *Nucleic Acids Res*.

Gangwal K, Sankar S, Hollenhorst PC, Kinsey M, Haroldsen SC, Shah AA, Boucher KM, Watkins WS, Jorde LB, Graves BJ, et al. 2008. Microsatellites as EWS/FLI response elements in Ewing's sarcoma. *Proc Natl Acad Sci U S A* **105**: 10149–10154.

Gorthi A, Romero JC, Loranc E, Cao L, Lawrence LA, Goodale E, Iniguez AB, Bernard X, Masamsetti VP, Roston S, et al. 2018. EWS-FLI1 increases transcription to cause R-Loops and block BRCA1 repair in Ewing sarcoma. *Nature* **555**: 387–391.

Grünewald TGP, Cidre-Aranaz F, Surdez D, Tomazou EM, De Álava E, Kovar H, Sorensen PH, Delattre O, Dirksen U. 2018. Ewing sarcoma. *Nat Rev Dis Prim* **4**: 5. http://www.nature.com/articles/s41572-018-0003-x.

Guo YE, Manteiga JC, Henninger JE, Sabari BR, Dall'Agnese A, Hannett NM, Spille JH, Afeyan LK, Zamudio A V., Shrinivas K, et al. 2019. Pol II phosphorylation regulates a switch between transcriptional and splicing condensates. *Nature*.

Johnson KM, Mahler NR, Saund RS, Theisen ER, Taslim C, Callender NW, Crow JC, Miller KR, Lessnick SL. 2017. Role for the EWS domain of EWS/FLI in binding GGAA-microsatellites required for Ewing sarcoma anchorage independent growth. *Proc Natl Acad Sci* **114**: 9870–9875.

Kato M, Han TW, Xie S, Shi K, Du X, Wu LC, Mirzaei H, Goldsmith EJ, Longgood J, Pei J, et al. 2012. Cell-free formation of RNA granules: Low complexity sequence domains form dynamic fibers within hydrogels. *Cell* **149**: 753–767.

Kato M, McKnight SL. 2018. A Solid-State Conceptualization of Information Transfer from Gene to Message to Protein. *Annu Rev Biochem* **87**: 351–390.

Kawaguchi T, Rollins MG, Moinpour M, Morera AA, Ebmeier CC, Old WM, Schwartz JC. 2020. Changes to the TDP-43 and FUS Interactomes Induced by DNA Damage. *J Proteome Res* **19**: 360–370. https://pubs.acs.org/doi/10.1021/acs.jproteome.9b00575.

Kovar H, Aryee DNT, Jug G, Henöckl C, Schemper M, Delattre O, Thomas G, Gadner H. 1996.

EWS/FLI-1 antagonists induce growth inhibition of Ewing tumor cells in vitro. *Cell Growth Differ* **7**: 429–437.

Kwon I, Kato M, Xiang S, Wu L, Theodoropoulos P, Mirzaei H, Han T, Xie S, Corden JL, McKnight SL. 2013. XPhosphorylation-regulated binding of RNA polymerase II to fibrous polymers of low-complexity domains. *Cell* **155**: 1049.

Lin Y, Currie SL, Rosen MK. 2017. Intrinsically disordered sequences enable modulation of protein phase separation through distributed tyrosine motifs. *J Biol Chem* **292**: 19110–19120.

Lin Y, Protter DSW, Rosen MK, Parker R. 2015. Formation and Maturation of Phase-Separated Liquid Droplets by RNA-Binding Proteins. *Mol Cell* **60**: 208–219.

Masuda A, Takeda JI, Okuno T, Okamoto T, Ohkawara B, Ito M, Ishigaki S, Sobue G, Ohno K. 2015. Position-specific binding of FUS to nascent RNA regulates mRNA length. *Genes Dev* **29**: 1045–1057.

McSwiggen DT, Hansen AS, Teves SS, Marie-Nelly H, Hao Y, Heckert AB, Umemoto KK, Dugast-Darzacq C, Tjian R, Darzacq X. 2019a. Evidence for DNA-mediated nuclear compartmentalization distinct from phase separation. *Elife*.

McSwiggen DT, Mir M, Darzacq X, Tjian R. 2019b. Evaluating phase separation in live cells: diagnosis, caveats, and functional consequences. *Genes Dev*.

Miller HE, Gorthi A, Bassani N, Lawrence LA, Iskra BS, Bishop AJR. 2020. Reconstruction of ewing sarcoma developmental context from mass-scale transcriptomics reveals characteristics of ewsr1-fli1 permissibility. *Cancers (Basel)*.

Molliex A, Temirov J, Lee J, Coughlin M, Kanagaraj AP, Kim HJ, Mittag T, Taylor JP. 2015. Phase Separation by Low Complexity Domains Promotes Stress Granule Assembly and Drives Pathological Fibrillization. *Cell*.

Moore MJ, Proudfoot NJ. 2009. Pre-mRNA Processing Reaches Back toTranscription and Ahead to Translation. *Cell* **136**: 688–700.

Murray DT, Kato M, Lin Y, Thurber KR, Hung I, McKnight SL, Tycko R. 2017. Structure of FUS Protein Fibrils and Its Relevance to Self-Assembly and Phase Separation of Low-Complexity Domains. *Cell* **171**: 615-627.e16.

Ozdilek BA, Thompson VF, Ahmed NS, White CI, Batey RT, Schwartz JC. 2017. Intrinsically disordered RGG/RG domains mediate degenerate specificity in RNA binding. *Nucleic Acids Res* **45**: 7984–7996.

Qamar S, Wang GZ, Randle SJ, Ruggeri FS, Varela JA, Lin JQ, Phillips EC, Miyashita A, Williams D, Ströhl F, et al. 2018. FUS Phase Separation Is Modulated by a Molecular Chaperone and Methylation of Arginine Cation-π Interactions. *Cell* **173**: 720-734.e15.

Riback JA, Zhu L, Ferrolino MC, Tolbert M, Mitrea DM, Sanders DW, Wei MT, Kriwacki RW, Brangwynne CP. 2020. Composition-dependent thermodynamics of intracellular phase separation. *Nature*.

Riggi N, Cironi L, Suvà M-L, Stamenkovic I. 2007. Sarcomas: genetics, signalling, and cellular origins. Part 1: The fellowship of TET. *J Pathol* **213**: 4–20.

Riggi N, Knoechel B, Gillespie SM, Rheinbay E, Boulay G, Suvà ML, Rossetti NE, Boonseng WE, Oksuz O, Cook EB, et al. 2014. EWS-FLI1Utilizes Divergent Chromatin Remodeling Mechanisms to Directly Activate or Repress Enhancer Elements in Ewing Sarcoma. *Cancer Cell* **26**: 668–681.

Sankar S, Gomez NC, Bell R, Patel M, Davis IJ, Lessnick SL, Luo W. 2013. EWS and RE1-Silencing Transcription Factor Inhibit Neuronal Phenotype Development and Oncogenic Transformation in Ewing Sarcoma. *Genes and Cancer*.

Sankar S, Lessnick SL. 2011. Promiscuous partnerships in Ewing's sarcoma. *Cancer Genet* **204**: 351–365. http://www.ncbi.nlm.nih.gov/pubmed/21872822.

Schwartz JC, Cech TR, Parker RR. 2015. Biochemical Properties and Biological Functions of FET Proteins. *Annu Rev Biochem* **84**: 355–379.

Schwartz JC, Ebmeier CC, Podell ER, Heimiller J, Taatjes DJ, Cech TR. 2012. FUS binds the CTD of

RNA polymerase II and regulates its phosphorylation at Ser2. *Genes Dev* **26**: 2690–2695.

Schwartz JC, Wang X, Podell ER, Cech TR. 2013. RNA Seeds Higher-Order Assembly of FUS Protein. *Cell Rep* **5**: 918–925.

Selvanathan SP, Graham GT, Erkizan H V, Dirksen U, Natarajan TG, Dakic A, Yu S, Liu X, Paulsen MT, Ljungman ME, et al. 2015. Oncogenic fusion protein EWS-FLI1 is a network hub that regulates alternative splicing. *Proc Natl Acad Sci U S A* **112**: E1307-16. https://www.ncbi.nlm.nih.gov/pubmed/25737553.

Selvanathan SP, Graham GT, Grego AR, Baker TM, Hogg JR, Simpson M, Batish M, Crompton B, Stegmaier K, Tomazou EM, et al. 2019. EWS–FLI1 modulated alternative splicing of ARID1A reveals novel oncogenic function through the BAF complex. *Nucleic Acids Res* **47**: 9619–9636.

Shannon P, Markiel A, Ozier O, Baliga NS, Wang JT, Ramage D, Amin N, Schwikowski B, Ideker T. 2003. Cytoscape: A software Environment for integrated models of biomolecular interaction networks. *Genome Res*.

Smith R, Owen LA, Trem DJ, Wong JS, Whangbo JS, Golub TR, Lessnick SL. 2006. Expression profiling of EWS/FLI identifies NKX2.2 as a critical target gene in Ewing's sarcoma. *Cancer Cell* **9**: 405–416.

Spahn L, Petermann R, Siligan C, Schmid JA, Aryee DNT, Kovar H. 2002. Interaction of the EWS NH2 terminus with BARD1 links the Ewing's sarcoma gene to a common tumor suppressor pathway. *Cancer Res* **62**: 4583–4587.

Spahn L, Siligan C, Bachmaier R, Schmid JA, Aryee DNT, Kovar H. 2003. Homotypic and heterotypic interactions of EWS, FLI1 and their oncogenic fusion protein. *Oncogene* **22**: 6819–6829.

Springhower CE, Rosen MK, Chook YM. 2020. Karyopherins and condensates. *Curr Opin Cell Biol*.

Stewart E, Goshorn R, Bradley C, Griffiths LM, Benavente C, Twarog NR, Miller GM, Caufield W, Freeman 3rd BB, Bahrami A, et al. 2014. Targeting the DNA repair pathway in Ewing sarcoma. *Cell Rep* **9**: 829–841. http://www.ncbi.nlm.nih.gov/pubmed/25437539.

Stoll G, Surdez D, Tirode F, Laud K, Barillot E, Zinovyev A, Delattre O. 2013. Systems biology of Ewing sarcoma: A network model of EWS-FLI1 effect on proliferation and apoptosis. *Nucleic Acids Res*.

Tan AY, Manley JL. 2009. The TET family of proteins: Functions and roles in disease. *J Mol Cell Biol* **1**: 82–92.

Theisen ER, Pishas KI, Saund RS, Lessnick SL. 2016. Therapeutic opportunities in Ewing sarcoma: EWS-FLI inhibition via LSD1 targeting. *Oncotarget* **7**: 17616–17630. https://www.ncbi.nlm.nih.gov/pubmed/26848860.

Thompson VF, Victor RA, Morera AA, Moinpour M, Liu MN, Kisiel CC, Pickrel K, Springhower CE, Schwartz JC. 2018. Transcription-Dependent Formation of Nuclear Granules Containing FUS and RNA Pol II. *Biochemistry* **57**: 7021–7032.

Tirode F, Surdez D, Ma X, Parker M, Le Deley MC, Bahrami A, Zhang Z, Lapouble E, Grossetete-Lalami S, Rusch M, et al. 2014. Genomic landscape of Ewing sarcoma defines an aggressive subtype with co-association of STAG2 and TP53 mutations. *Cancer Discov* **4**: 1342–1353. http://www.ncbi.nlm.nih.gov/pubmed/25223734.

Trapnell C, Roberts A, Goff L, Pertea G, Kim D, Kelley DR, Pimentel H, Salzberg SL, Rinn JL, Pachter L. 2012. Differential gene and transcript expression analysis of RNA-seq experiments with TopHat and Cufflinks. *Nat Protoc*.

Vo KT, Edwards J V, Epling CL, Sinclair E, Hawkins DS, Grier HE, Janeway KA, Barnette P, McIlvaine E, Krailo M, et al. 2016. Impact of Two Measures of Micrometastatic Disease on Clinical Outcomes in Patients with Newly Diagnosed Ewing Sarcoma: A Report from the Children's Oncology Group. *Clin Cancer Res*. http://www.ncbi.nlm.nih.gov/pubmed/26861456.

Wang J, Choi JM, Holehouse AS, Lee HO, Zhang X, Jahnel M, Maharana S, Lemaitre R, Pozniakovsky A, Drechsel D, et al. 2018. A Molecular Grammar Governing the Driving Forces for Phase Separation of Prion-like RNA Binding Proteins. *Cell* **174**: 688-699.e16.

Wei M-T, Chang Y-C, Shimobayashi SF, Shin Y, Strom AR, Brangwynne CP. 2020. Nucleated transcriptional condensates amplify gene expression. *Nat Cell Biol* 1–10. http://www.nature.com/articles/s41556-020-00578-6 (Accessed September 17, 2020).

Zamudio A V., Dall'Agnese A, Henninger JE, Manteiga JC, Afeyan LK, Hannett NM, Coffey EL, Li CH, Oksuz O, Sabari BR, et al. 2019. Mediator Condensates Localize Signaling Factors to Key Cell Identity Genes. *Mol Cell*.

## FIGURE LEGENDS

**Figure 1. A large number of transcripts respond similarly to the loss of EWS-FLI1 or EWSR1 in Ewing sarcoma.** (**A**) Schematic (*top*) shows locations in *EWSR1* or *EWS-FLI1* mRNA targeted by siRNA. Real-time PCR analysis shows average knockdown in A673 cells by siRNA transfections targeting EWS-FLI1 (siEF), EWSR1 (siEWSR1) or both (siE-EF) relative to negative controls. Error bars represent standard error about the mean. (**B**) A heat map shows fold changes for the 123 signature genes repressed by EWS-FLI1. Results are sorted according to change in the siEF treatment and genes names for the top 40 genes are listed. Published data from Ref. #1 is a stable shRNA knockdown of EWS-FLI1 in A673 cells (Sankar et al. 2013). Published data from Ref. #2 is a stable shRNA knockdown of EWS-FLI1 in A673 or SKNMC cells (Riggi et al. 2014). (**B**) A comparison of cells treated with siEF or siEWSR1 revealed a similar increase or decrease in abundance by >1.8-fold for 439 transcripts (green) and in the opposite directions for 46 transcripts (yellow). The number of transcripts changed >1.8-fold are indicated in each quartile. (**C**) Publicly available data (GEO Accession: GSE98836) was analyzed for an EWSR1 knockdown by siRNA (siEWS) in HeLa cells. A comparison of affected HeLa gene transcripts and A673 genes shown in green for part B (N↑↑ + N↓↓) identified 92 genes changed by an EWSR1 knockdown in both cell lines, as well as for the EWS-FLI1 knockdown in A673 cells. (**D**) Genes similarly affected by siEWSR1 and siEF (N↑↑ + N↓↓) were compared to affected genes for the stable EWS-FLI1 knockdowns in A673 to identify 206 genes affected across all A673 datasets. A selection of significant Gene Ontology associations is shown from a network analysis of the 206 intersecting genes. Terms are ranked by significance, as shown by the $-LOG_{10}$ of the corrected p-values.

**Figure 2. Loss of EWSR1 inhibits anchorage-independent growth in Ewing sarcoma cells.** (**A**) Left, western assays reveal knockdown for EWSR1 or EWS-FLI1 in A673 cells for treatment with siSCR, siEF, or siEWSR1. Right, averaged levels of protein were determined by densitometry relative to siSCR treatments (n = 3). (**B**) Left, soft agar assays were performed with A673 cells treated with siSCR, siEF, or siEWSR1. Right, colonies were counted to reveal reductions in averaged values relative to siSCR treatment (n = 3). (**C**) Left, western assays reveal knockdown for EWSR1 or EWS-FLI1 in HEK293T/17 cells for treatment with siSCR, siEF, or siEWSR1. Right, averaged levels of protein were determined by densitometry relative to siSCR treatments (n = 4). (**D**) Left, soft agar assays were performed for HEK293T/17 cells treated with siSCR, siEF, or siEWSR1. Right, colonies were counted

to reveal no change in averaged values relative to siSCR treatment (n = 4). All error bars represent standard deviation. Student's *t*-test was calculated assuming equal variances: ** $p < 0.01$; * $p < 0.05$; n.s., not significant ($p > 0.05$).

**Figure 3. EWS-FLI1 can alter effects on cell growth for an EWSR1 knockdown.** (**A**) Left, growth on soft agar was assessed for HEK293T/17 cells after transfection of empty plasmids or a plasmid expressing V5-EWS-FLI1. Right, colonies were counted to reveal no change in averaged values relative to siSCR treatment (n = 4). (**B**) Left, soft agar assays were performed with HEK293T/17 cells expressing V5-EWS-FLI1 and co-transfected with siSCR or siEWSR1 (n = 6). Right, colonies were counted to reveal a reduction in averaged values relative to siSCR treatment . Error bars represent standard deviation. Student's *t*-test was calculated for assuming equal variances: *** $p < 0.001$.

**Figure 4. EWSR1 and RNA Pol II are assembled in large protein assemblies.** (**A**) Total protein from HEK293T/17 cell lysates was analyzed by SEC to separate proteins, complexes, or assemblies by size. The averaged ELISA signals are shown normalized to their maximum values for EWSR1 (C-9 antibody), yellow, or RNA Pol II (CTD4H8 antibody), red, as measured by ELISA. For samples from cells not crosslinked, top, RNA Pol II signals were highest in fractions eluting just before 20 mL, corresponding to particles of 25 nm in size. EWSR1 eluted after 20 mL or as a particle < 25 nm in size. For crosslinked samples, bottom, the elution of EWSR1 and RNA Pol II shifted to early fractions with particles measured to be up to 150 nm in diameter. Dashed lines represent standard error about the mean (n = 3). (**B**) IP assays using cells without crosslinking enrich for ordinary and stable molecular complexes. Those using crosslinked cells can recover large molecular assemblies that form by weak protein interactions. (**C**) Left, ELISA assays detected EWSR1 eluted from crosslinked IP assays of phosphorylated (S5P) RNA Pol II (Abcam, ab5131) in HEK293T/17 cells (n = 3). Right, S5P RNA Pol II was detected for crosslinked IP of EWSR1 (B-1 antibody) (n = 3). (**D**) Left, ELISA assays in A673 cells also detected EWSR1 eluted with S5P RNA Pol II. Right, S5P RNA Pol II was detected in crosslinked IP assays of EWSR1 (n = 3). All error bars represent standard error about the mean. AU = absorbance units. RLU = relative luminescence units. Student's *t*-test was calculated assuming equal variances: ** $p < 0.01$; * $p < 0.05$; *n.s.*, not significant ($p > 0.05$).

**Figure 5. EWS-FLI1 and RNA Pol II coimmunoprecipitate in crosslinked protein granules.** ELISA assays using an antibody to FLI1 measured interactions with FLI1-fusion proteins recovered by co-IP assays from crosslinked cells. The IP of EWSR1 (B-1) or RNA Pol II (CTD4H8) recovered V5-EWS-FLI1 (**A**) but not YS37 (**B**) protein expressed in HEK293T/17 cells by plasmid transfections (n = 3 each). (**C**) Crosslinked IP assays of EWSR1 and RNA Pol II also recovered endogenous EWS-FLI1 from A673 cells (n = 4). (**D**) Transmission electron microscopy detected protein particles recovered from crosslinked HEK293T/17 cells by IP of EWS-FLI1 (anti-FLI1 antibody, left) and RNA Pol II (CTD4H8, left), but not of YS37 (anti-FLI1 antibody, center). Scale bar inset represents 50 nm. Cumulative plots show diameters for particles imaged in IP samples for EWS-FLI1 (n = 24) or RNA Pol II (n = 77). All error bars represent standard error about the mean. Student's *t*-test was calculated assuming equal variances: ** $p < 0.01$; * $p < 0.05$; n.s., not significant ($p > 0.05$).